SUPPLEMENTARY INFORMATION

Two-Photon Absorption in Graphene Enhanced by the Excitonic Fano Resonance

Weiqiang Chen[1], Yu Wang[2,]*, and Wei Ji[1,]*

[1]Department of Physics, National University of Singapore, 2 Science Drive 3, Singapore, 117542

[2]State Key Laboratory of Multiphase Complex Systems, Institute of Process Engineering, Chinese Academy of Sciences, Beijing 100190, P. R. China

Supplementary Text, Figures and Legends **S1-8**, Tables **S1-3**

*To whom the correspondence should be addressed.   Email: phyjiwei@nus.edu.sg and wyu@home.ipe.ac.cn

SI. Characterization of the CVD-grown graphene films

SI-1. Optical microscopic and SEM images of the graphene films

The homogeneity of the CVD-grown 5-layer and superimposed 10-layer graphene films on quartz was examined in detail by using an optical microscope (Nikon Eclipse Ti with a 50× objective lens). Figures S1a and S1b display two images that were zoomed on the edges of the 5- and 10-layer graphene films, respectively. They clearly show the continuous smoothness of the graphene films. Before the films were transferred onto quartz substrate, they were also examined by a scanning electron microscope (SEM, Nova nanoSEM 230) for quality control. Figure S1c presents such a SEM image of the 5-layer graphene on the copper foil, showing the desirable features of a continuous even surface. The insets in Figure S1d depict the photos of the 5-layer and 10-layer graphene films on a large scale.
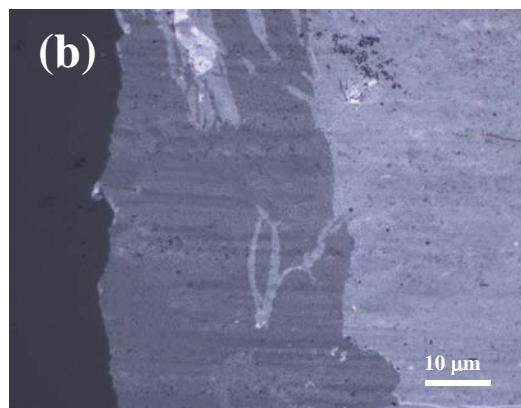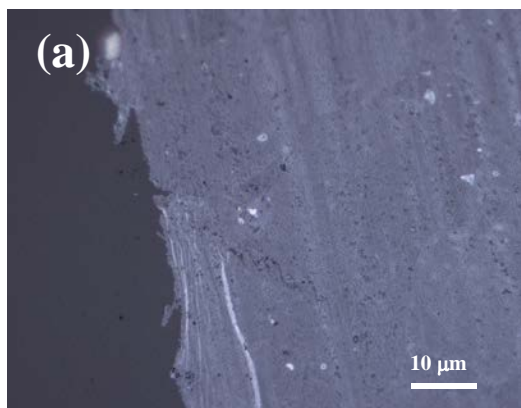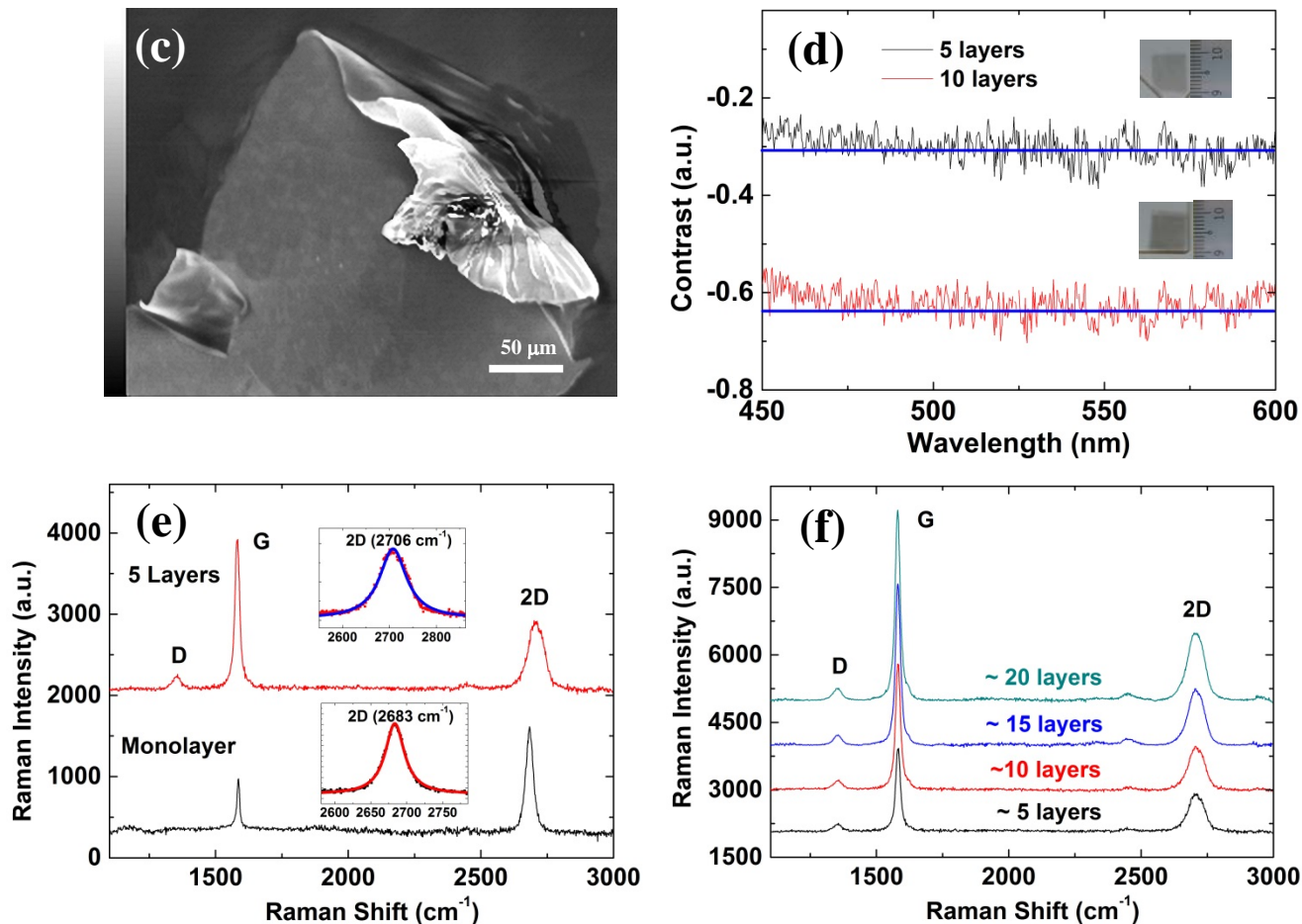
Figure S1. (a) and (b) show the optical microscopic images of the 5- and 10-layer graphene films on quartz, respectively; (c) displays the SEM image of the 5-layer graphene film on copper foil; (d) shows the reflection contrast spectra of the 5- and 10-layer graphene films on quartz, and insets show their large-scale optical images; (e) shows the micro-Raman spectra of the monolayer (black) and 5-layer (red) graphene films on quartz; and (f) displays the micro-Raman spectra of the 5-layer (black), 10-layer (red), 15-layer (blue), and 20-layer (dark cyan) graphene films on quartz.

SI-2. Micro-Raman spectra of the 1-, 5- and 10-layer graphene films

A micro-Raman spectrometer (WITec Alpha300 R with a laser wavelength of 532 nm, 50× objective lens) was employed to characterize the crystalline quality of the synthesised graphene films. Because the graphene films have a size of ~ 8×10 mm^2, we randomly selected 10 areas of 1×1 mm^2 on every film for micro-Raman inspection to ensure their spatial uniformity. (These areas were also used in the experiments described in the following **Sections**, and in the **main text**) No significant difference in these Raman spectra was found, indicating a high spatial uniformity.

The black curve in Figure S1e displays a representative micro-Raman spectrum of the monolayer graphene film transferred to quartz substrate. Two primary features are pronounced in all the spectra, including (i) a G peak located at ~ 1580 cm^{-1} caused by the in-plane optical vibration (degenerate zone center E_{2g} mode) and (ii) a 2D peak located at ~ 2700 cm^{-1} corresponding to the second-order zone boundary phonons, close to reported values.[1-7] We find that the 2D to G peak intensity ratio I_{2D}/I_G of the Raman spectrum is ~ 2.1 and the full width at half-maximum (FWHM) of its symmetric 2D band (single-Lorentzian profile as shown in the bottom inset of Figure S1e) is ~ 32 cm^{-1}. Both these two features were studied before[1-7] and support that the graphene is single layer. The absence of the disorder-induced D peak (~ 1350 cm^{-1}) indicates very low defect density and very high crystalline quality in the monolayer graphene film as reported by Ref. [1,8]. The red curve in Figure S1e shows an increase in G peak and also a decrease in 2D peak, indicating the formation of multilayer graphene, similar to previous results[2-4,6,7] on CVD graphene. Moreover, the 2D to G peak intensity ratio I_{2D}/I_G becomes ~ 0.45 < 1 and the FWHM of the symmetric 2D band is ~ 70 cm^{-1}, revealing that the

layer number of the multilayer graphene film should be larger than three. [2-4,6,7] This finding is also consistent with the experimental data in **Section SI-3**.

Although a weak disorder-induced D peak is observed in the 5-layer graphene film, the typical D to G intensity ratio I_D/I_G is ~ 0.09 < 0.1, indicating both low density of defects and high crystalline quality.[2-7] Despite its multilayer nature, however, we did not observe the multi-peaked and "shouldered" 2D peak in the 5-layer graphene film, which is the hallmark of HOPG-mechanically exfoliate multilayer graphene samples and results from strong interlayer coupling.[1,4,8-10] Furthermore, the 2D peak shows a single-Lorentzian line shape as demonstrated in the top inset of Figure S1e. These experimental data support that interlayer coupling is so weak that can be neglected in the 5-layer graphene film.[2,4,8] The 5-layer graphene film resembles multilayer turbostratic graphene with turbostratic random stacking.[4,11,12] Therefore, such a 5-layer graphene film exhibits electronic properties similar to those of a single-layer graphene.[2,4,8,11-13] In addition, its 2D peak has a slight up-shift (~ 20 cm^{-1}) relative to that of the monolayer graphene, similar to the previous Raman spectra on CVD-grown multilayer graphene[2-4,6,7] and turbostratic graphite,[14] further demonstrating the insignificance of interlayer coupling. Our conclusion is consistent with many reports [2,4,11,12] that weak interlayer coupling (and the resultant symmetry of the 2D peak) is a common feature of CVD-grown multilayer graphene.

As comparison, the micro-Raman spectra of the superimposed 10-, 15-, and 20-layer graphene films are shown in Figure S1f, together with that of the 5-layer graphene film. As the 5-layer graphene films are stacked sequentially,[5,7,15] the intensities of the G- and 2D-band peaks increase, but no significant change in the G to 2D ratios was found, similar to the previous report on CVD graphene.[5] This supports that there is nearly-zero interlayer coupling between the 5-

layer graphene films. As such, the electronic properties of the superimposed 10-, 15-, and 20-layer graphene films are also similar to those of a single-layer of graphene.[5,13,16]

SI-3. Reflection contrast spectroscopy of the 5- and 10-layer graphene films

Reflection contrast spectroscopy[17,18] was utilized to characterize the thickness (or layer number) of the CVD-grown multilayer graphene films. The reflection spectra, $R_0(\lambda)$, from bare quartz substrate and $R(\lambda)$ from graphene sheet on quartz substrate were measured with an optical microscope (Nikon Eclipse Ti), a white light source (tungsten halogen lamp) and a spectrometer (Avaspec-2048-SPU). A 50× objective lens with a numerical aperture of 0.80 was used and the spot size of the white light was estimated to be ~ 1.5 μm determined by a scanning edge method.[19] The reflected light was collected by using backscattering configuration. The contrast spectra, $C(\lambda)$, are defined by:[17,18]

$$C(\lambda) = \frac{R_0(\lambda) - R(\lambda)}{R_0(\lambda)} \qquad (1)$$

It was reported [20,21] that the contrast values are around $N \times (-0.068)$ for multilayer graphene (N = 1, 2, ..., to 10) on quartz substrate. Figure S1d shows two examples for the contrast spectra of our graphene films (N = 5 and N = 10) on quartz. The contrast spectra are nearly flat in the spectral range of 450-600 nm, similar to the previous reports.[20,21] By comparison between our contrast values (-0.31 and -0.63) and the reported values in Ref. [20,21], the layer number of the graphene films was determined to be 5 and 10, respectively.

Furthermore, the 1PA spectra of the 5- and 10-layer graphene films on the quartz were also measured and two of the spectra are shown in the Figure 1 of the **main text**. It is known that

single-layer graphene should absorb an amount of 2.3% of incident light power across the NIR spectral region.[22,23] By comparing the percentage of absorbed NIR light power in the multilayer graphene with the single-layer value of 2.3%, the number of graphene layers was obtained and found to be consistent with the results from the above-said reflection contrast spectroscopy.

## SII.   Z-scans on the 1-, 5-, 10-, 15-, and 20-layer graphene films

SII-1. Z-scans on the 1-layer graphene film at 800 and 535 nm

Figures S2a,b display the measured Z-scans on the 1-layer graphene sample at 800 and 535 nm and under laser pulses excitation of various peak intensities (I_{00}). (The definition of I_{00} can be found in the **main text**.)

Both optical microscopic images and AFM images (Figures S2c-j) of the focal spots on the 1-layer graphene sample taken before and after these Z-scans show no damage was induced by the laser illumination (0.4 - 20 GW/cm^2). Figure S2k displays the optical microscopic image of the sample edge between graphene and quartz substrate to help us identify the single-layer graphene on quartz. We acquired the optical microscopic images utilizing the Nikon Eclipse Ti optical microscope with a 50× objective lens, and the AFM images were obtained in the tapping mode of the atomic force microscopy (AFM, BRUKER Dimension FastScan). Relative displacement from one of the quartz corners to the focal spot was recorded to make sure that the optical and AFM images were acquired on the laser focal spot.
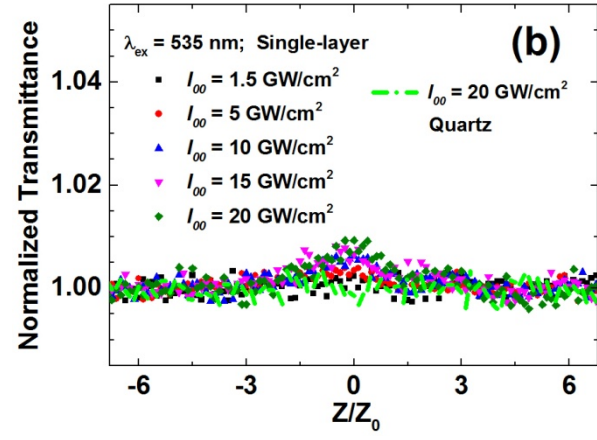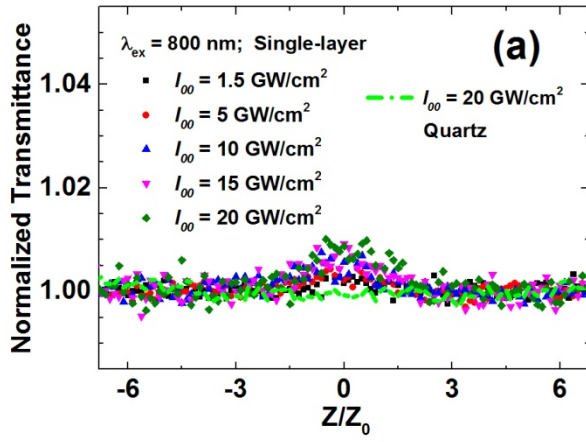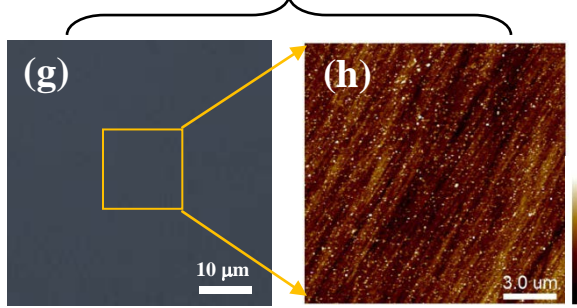
Single-layer: λ_{ex} = 800 nm before Z-scan
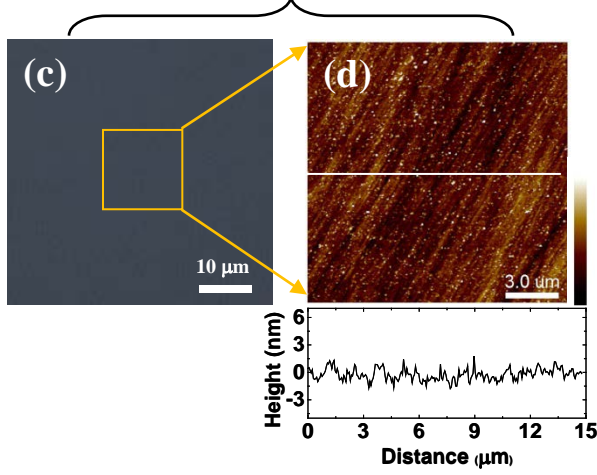
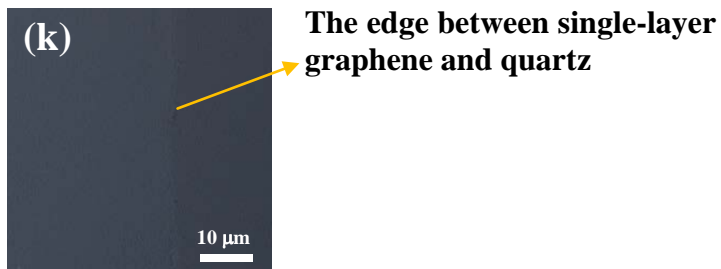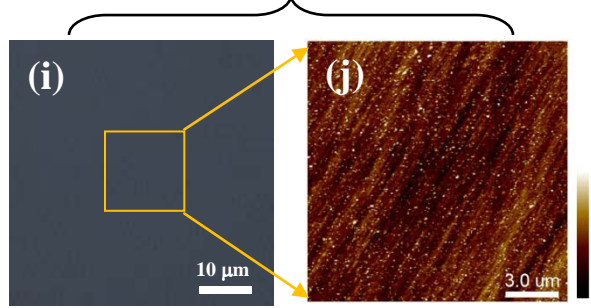Single-layer: λ_{ex} = 800 nm after Z-scan

Single-layer: λ_{ex} = 535 nm before Z-scan

Single-layer: λ_{ex} = 535 nm after Z-scan

The edge between single-layer graphene and quartz
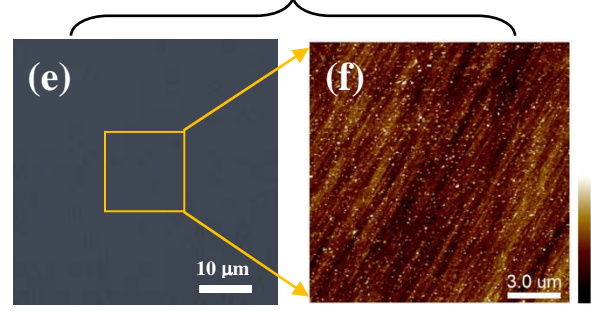
Figure S2. (a,b) Open-aperture Z-scans on the 1-layer graphene sample at 800 and 535 nm, respectively. The symbols are the experimental data at various values of I_{00}. The green lines are Z-scans on quartz substrate at $I_{00} = 20$ GW/cm^2. (c-j) The optical microscopic and AFM images of the focal spot on the 1-layer graphene sample on quartz before and after the Z-scans, the height profile below figure (d) is corresponding to the white-line. (k) The optical microscopic image of the sample edge between 1-layer graphene and quartz substrate.

SII-2. Z-scans on the 10-layer graphene film at selected wavelengths in the range from 435 to 1100 nm

The open-aperture Z-scans were carried out with femtosecond laser pulses on one of the ten areas (1 × 1 mm^2) of the 10-layer graphene film. Figure S3 displays the measured Z-scans on the graphene film at selected wavelengths in the range from 435 to 1100 nm and with various peak intensities (I_{00}) of the excitation laser pulses. (The definition of I_{00} can be found in the **main text**.) In Figure S3, the colored symbols are the measured Z-scan data. From these measured Z-scans, we obtained their corresponding plots of normalized transmittance change ($\Delta T/T_0$) at $z = 0$ as a function of I_{00}, as displayed by the symbols in Figure S4. The solid curves in Figures S3 and S4 are the modeling of $\alpha = \alpha_0/[1+I/I_s] + \beta I$, (see eq. 2 in the **main text**), where $\alpha_0 = N\alpha_{mono}$, α_{mono} is the 1PA coefficient of single-layer graphene, N is the layer number, $\beta = \beta_{mono} N^2 / (1+0.023N/2)^8$, and β_{mano} is the 2PA coefficient of single-layer graphene. On the other hand, the dashed curves in Figure S4 are the modeling of the above equation without the 2PA term using $\alpha = \alpha_0/[1+I/I_s]$ and $\beta = 0$. The parameters used in the modeling to fit the experimental data in Figures S3 and S4 are listed in Table S1. Here, the experimental error of 10-15% results mainly from the uncertainty in fluctuation of input laser pulse energy and determination of laser beam characteristics such as minimum beam waist and pulse duration.
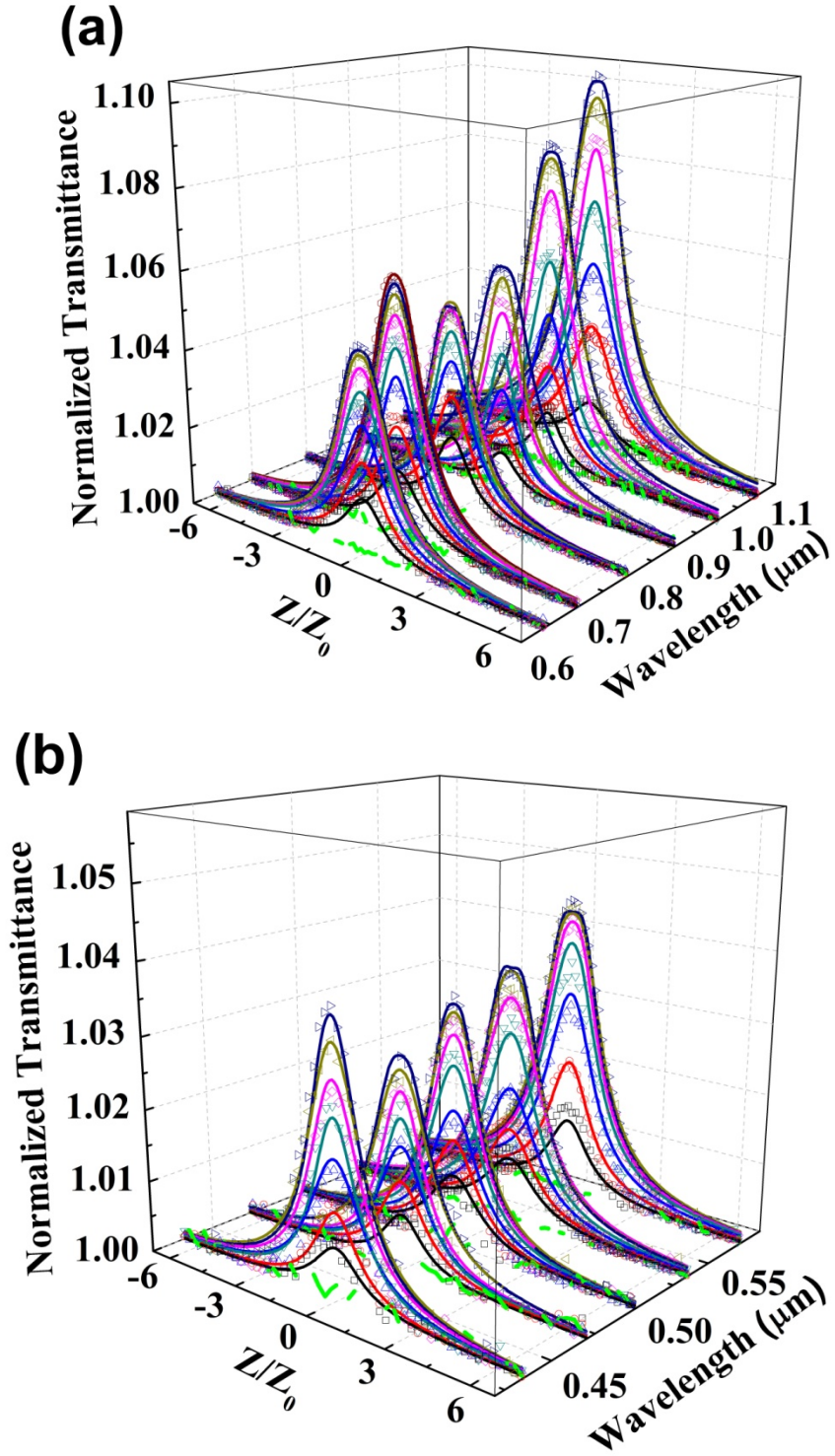
Figure S3. Z-scans on the 10-layer graphene sample at selected wavelengths in the range (a) from 1100 to 640 nm and (b) from 575 to 435 nm. The symbols are the experimental data at

various values of I_{00}. The solid curves are the theoretical fits based on eq. 2 in the main text. The green lines are Z-scans on quartz substrate at $I_{00} = 20$ GW/cm^2.
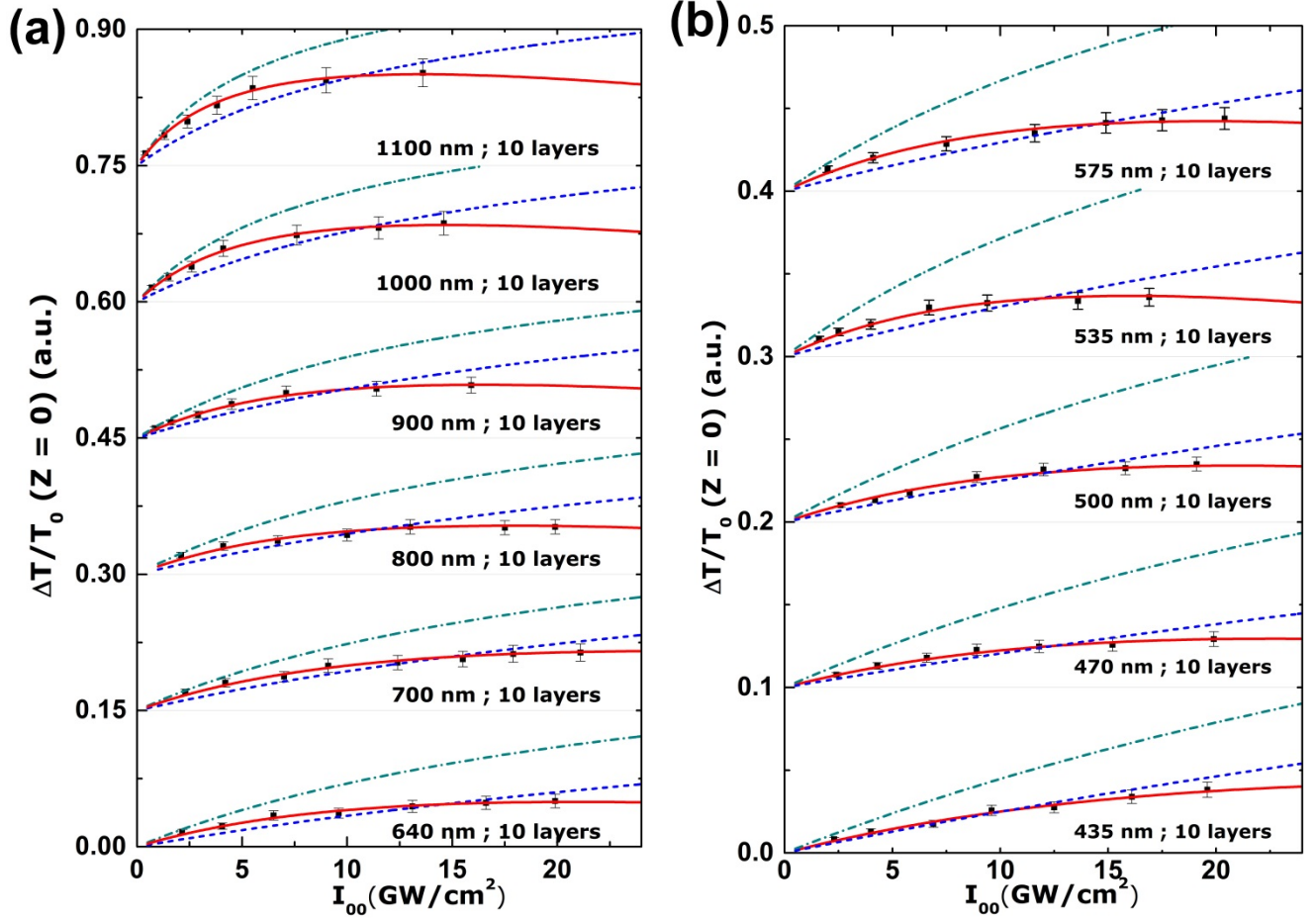
Figure S4. Plots of $\Delta T/T_0$ vs. I_{00} at $z = 0$. The symbols are the experimental data at various values of I_{00}. The solid and dashed curves are the modeling with $\beta \neq 0$ and $= 0$, respectively.

Table S1. Fitting parameters used in the modeling of Z-scans on the 10-layer graphene sample at selected wavelengths in the range from 1100 to 435 nm as in Figure S3 and their corresponding plots of $\Delta T/T_0$ vs. I_{00} at $z = 0$ as in Figure S4.

Fitting Wavelength		—— (red)	— · — (green)	— — — (blue)
1100 nm	$\alpha_{mono} =$ $7.1 \pm 0.8 \times 10^{-5}$ cm^{-1}	$I_s = 2.3 \pm 0.3$ GW/cm^2 $\beta_{mono} = 0.86 \pm 0.09$ cm/MW	$I_s = 2.3 \pm 0.3$ GW/cm^2 $\beta_{mono} = 0$	$I_s = 4.7 \pm 0.6$ GW/cm^2 $\beta_{mono} = 0$
1000 nm	$\alpha_{mono} =$ $7.2 \pm 0.8 \times 10^{-5}$ cm^{-1}	$I_s = 3.1 \pm 0.4$ GW/cm^2 $\beta_{mono} = 0.79 \pm 0.08$ cm/MW	$I_s = 3.1 \pm 0.4$ GW/cm^2 $\beta_{mono} = 0$	$I_s = 6.5 \pm 0.8$ GW/cm^2 $\beta_{mono} = 0$
900 nm	$\alpha_{mono} =$ $7.4 \pm 0.9 \times 10^{-5}$ cm^{-1}	$I_s = 5.7 \pm 0.7$ GW/cm^2 $\beta_{mono} = 0.69 \pm 0.07$ cm/MW	$I_s = 5.7 \pm 0.7$ GW/cm^2 $\beta_{mono} = 0$	$I_s = 11.0 \pm 1.4$ GW/cm^2 $\beta_{mono} = 0$
800 nm	$\alpha_{mono} =$ $7.7 \pm 0.9 \times 10^{-5}$ cm^{-1}	$I_s = 7.5 \pm 1.0$ GW/cm^2 $\beta_{mono} = 0.60 \pm 0.06$ cm/MW	$I_s = 7.5 \pm 1.0$ GW/cm^2 $\beta_{mono} = 0$	$I_s = 16.0 \pm 2.1$ GW/cm^2 $\beta_{mono} = 0$
700 nm	$\alpha_{mono} =$ $8.1 \pm 0.9 \times 10^{-5}$ cm^{-1}	$I_s = 9.0 \pm 1.2$ GW/cm^2 $\beta_{mono} = 0.43 \pm 0.05$ cm/MW	$I_s = 9.0 \pm 1.2$ GW/cm^2 $\beta_{mono} = 0$	$I_s = 17.0 \pm 2.2$ GW/cm^2 $\beta_{mono} = 0$
640 nm	$\alpha_{mono} =$ $8.4 \pm 1.0 \times 10^{-5}$ cm^{-1}	$I_s = 10.0 \pm 1.3$ GW/cm^2 $\beta_{mono} = 0.55 \pm 0.06$ cm/MW	$I_s = 10.0 \pm 1.3$ GW/cm^2 $\beta_{mono} = 0$	$I_s = 22.0 \pm 2.9$ GW/cm^2 $\beta_{mono} = 0$
575 nm	$\alpha_{mono} =$ $8.7 \pm 1.0 \times 10^{-5}$ cm^{-1}	$I_s = 13.0 \pm 1.7$ GW/cm^2 $\beta_{mono} = 0.67 \pm 0.07$ cm/MW	$I_s = 13.0 \pm 0.4$ GW/cm^2 $\beta_{mono} = 0$	$I_s = 29.0 \pm 3.8$ GW/cm^2 $\beta_{mono} = 0$
535 nm	$\alpha_{mono} =$ $9.1 \pm 1.0 \times 10^{-5}$ cm^{-1}	$I_s = 12.5 \pm 1.6$ GW/cm^2 $\beta_{mono} = 0.81 \pm 0.09$ cm/MW	$I_s = 12.5 \pm 1.6$ GW/cm^2 $\beta_{mono} = 0$	$I_s = 29.0 \pm 3.8$ GW/cm^2 $\beta_{mono} = 0$
500 nm	$\alpha_{mono} =$ $9.5 \pm 1.1 \times 10^{-5}$ cm^{-1}	$I_s = 17.0 \pm 2.2$ GW/cm^2 $\beta_{mono} = 0.62 \pm 0.07$ cm/MW	$I_s = 17.0 \pm 2.2$ GW/cm^2 $\beta_{mono} = 0$	$I_s = 41.0 \pm 5.3$ GW/cm^2 $\beta_{mono} = 0$
470 nm	$\alpha_{mono} =$ $9.9 \pm 1.1 \times 10^{-5}$ cm^{-1}	$I_s = 18.0 \pm 2.3$ GW/cm^2 $\beta_{mono} = 0.55 \pm 0.06$ cm/MW	$I_s = 18.0 \pm 2.3$ GW/cm^2 $\beta_{mono} = 0$	$I_s = 41.0 \pm 5.3$ GW/cm^2 $\beta_{mono} = 0$
435 nm	$\alpha_{mono} =$ $10.5 \pm 1.2 \times 10^{-5}$ cm^{-1}	$I_s = 21.5 \pm 2.8$ GW/cm^2 $\beta_{mono} = 0.36 \pm 0.04$ cm/MW	$I_s = 21.5 \pm 2.8$ GW/cm^2 $\beta_{mono} = 0$	$I_s = 40.0 \pm 5.2$ GW/cm^2 $\beta_{mono} = 0$

As shown clearly by Figure S4, the nonlinear signals ($\Delta T/T_0$) are dominated by 1PA saturation at relatively lower excitation ($I_{00} < 5$ GW/cm^2, or below the saturation intensity, I_s). However, the 2PA manifests itself in the higher excitation regime, which can be identified from the deviation of the measurements in Figure S4 from the dashed curves in the higher excitation

regime, demonstrating that both 1PA saturation and 2PA should contribute to the overall nonlinear signal.

From Table S1 and also Table S2 shown below, the saturation intensity is $I_s \sim 7.5 \pm 1.0$ GW/cm^2 at 800 nm, close to the experimentally measured values on epitaxial graphene,[24] and it is also on the same order of magnitude as the theoretical calculation.[25] This validates our Z-scan analysis.

SII-3. Z-scans on the 5-, 10-, 15-, and 20-layer graphene films at 800 and 535 nm

Figures S5a,b display the Z-scans (symbols) measured at 800 and 535 nm on the 5-, and superimposed 10-, 15- and 20-layer graphene films, respectively. Figures S6a,b show the corresponding plots of $\Delta T/T_0$ (at $z = 0$) vs. I_{00}. In Figures S5 and S6, the symbols are the experimental data, and the curves are the modeling. The fitting parameters are listed in Tables S2 and S3.

Figures S7a-p display both optical microscopic images and AFM images of the focal spots on the 5- and 10-layer graphene samples before and after the Z-scans at 800 and 535 nm. These images demonstrate no damage was induced by laser illumination during the Z-scans.
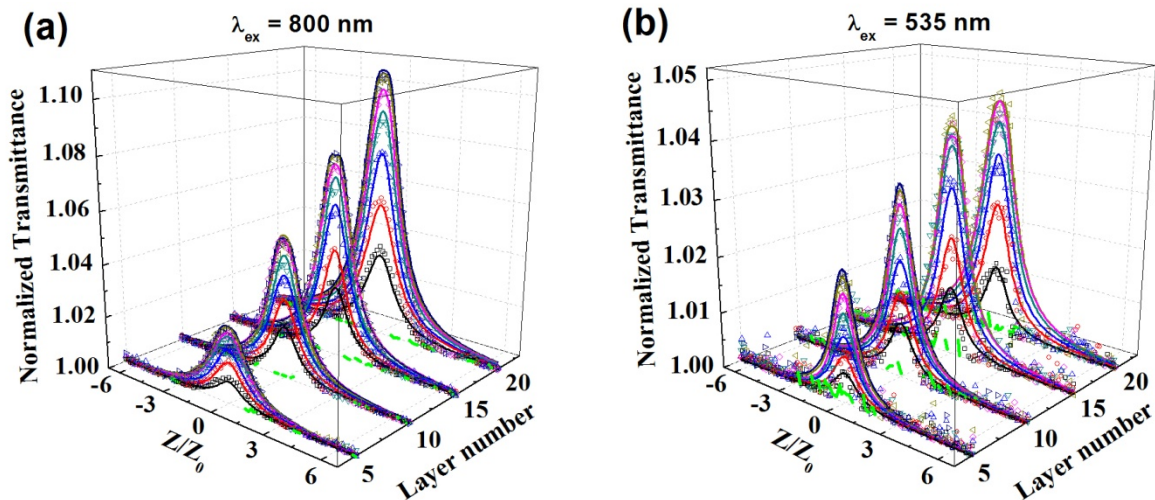
Figure S5. Open-aperture Z-scan measurements on the 5- and superimposed 10-, 15- and 20-layer CVD-grown graphene films on the quartz substrate at 800 and 535 nm. The symbols are the experimental Z-scan data at various values of I_{00}. The solid curves are the theoretical fits based on eq. 2 in the main text. The green lines are Z-scans on quartz substrate at $I_{00} = 20$ GW/cm^2.
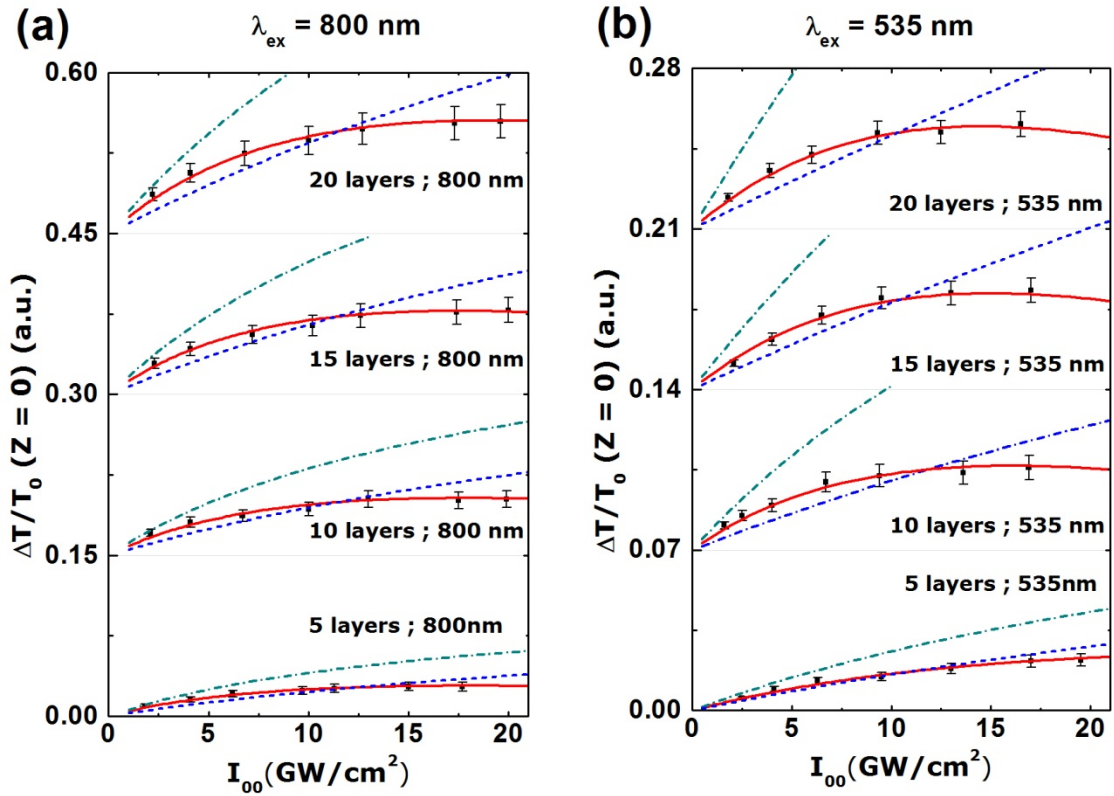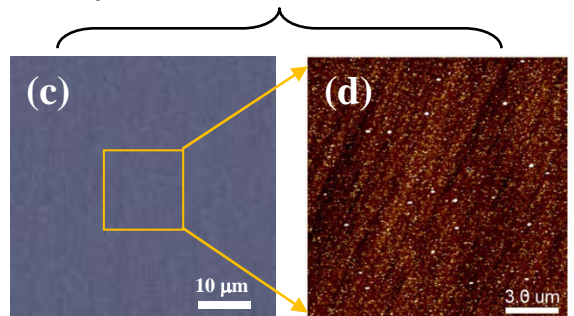

Figure S6. Plots of $\Delta T/T_0$ (at $z = 0$) vs. I_{00} corresponding to the Z-scan measurements in Figure S5. The symbols are the experimental data at various values of I_{00}. The solid and dashed curves are the modeling with and without the term of two-photon absorption, respectively.
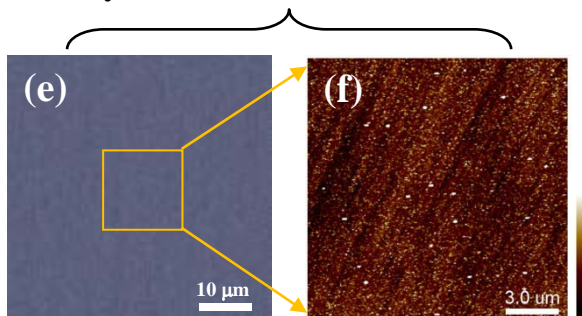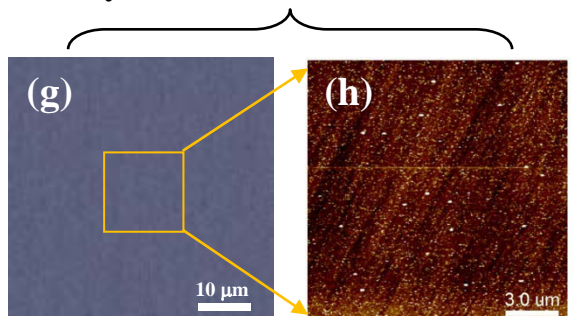
14

5-layer: λ_{ex} = 800 nm before Z-scan
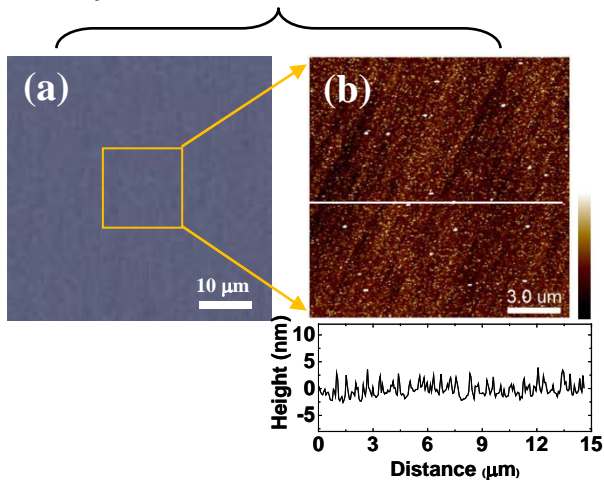
5-layer: λ_{ex} = 800 nm after Z-scan
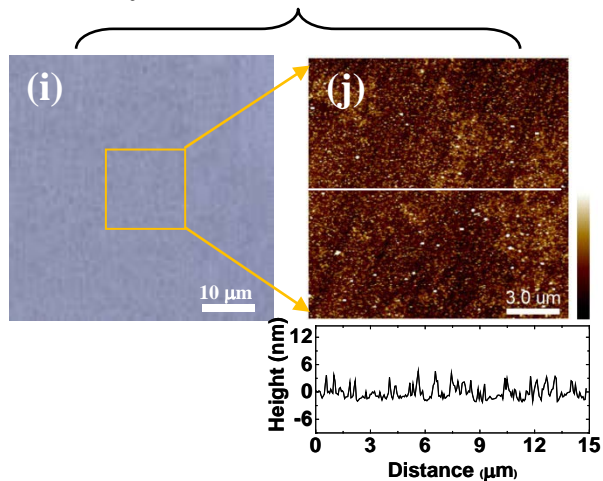

5-layer: λ_{ex} =535 nm before Z-scan

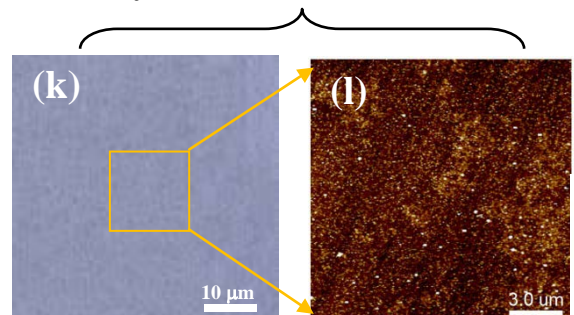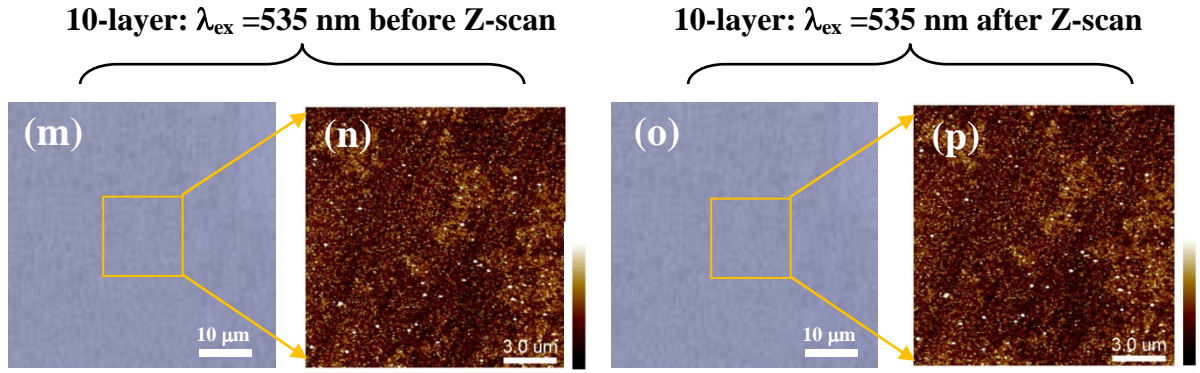**5-layer: λ_{ex} = 535 nm after Z-scan**

10-layer: λ_{ex} =800 nm before Z-scan

10-layer: λ_{ex} = 800 nm after Z-scan

15

10-layer: λ_{ex} =535 nm before Z-scan

10-layer: λ_{ex} =535 nm after Z-scan

Figure S7. (a-h) Both optical microscopic and AFM images of the focal spot on the 5-layer graphene sample on quartz before and after the Z-scans at 800 and 535 nm, the height profile below figure (b) is corresponding to the white-line. Note that the crossing line in the AFM image (h) is believed to be due to the experimental error from the set-up. (i-p) Both optical microscopic and AFM images of the focal spot on the 10-layer graphene sample on quartz before and after the Z-scans at 800 and 535 nm.

Table S2. Fitting parameters used in the modeling of Z-scans at 800 nm on 5, and superimposed 10-, 15- and 20-layer graphene samples as in Figure S5a and their corresponding plots of $\Delta T/T_0$ vs. I_{00} at $z = 0$ as in Figure S6a.

Fitting Layer Number		———	—·—	———
5 layers	$\alpha_{mono} =$ $7.5 \pm 0.9 \times 10^{-5}$ cm^{-1}	$I_s = 6.7 \pm 0.9$ GW/cm^2 $\beta_{mono} = 0.63 \pm 0.07$ cm/MW	$I_s = 6.7 \pm 0.9$ GW/cm^2 $\beta_{mono} = 0$	$I_s = 13.0 \pm 1.7$ GW/cm^2 $\beta_{mono} = 0$
10 layers	$\alpha_{mono} =$ $7.7 \pm 0.9 \times 10^{-5}$ cm^{-1}	$I_s = 7.5 \pm 1.0$ GW/cm^2 $\beta_{mono} = 0.60 \pm 0.06$ cm/MW	$I_s = 7.5 \pm 1.0$ GW/cm^2 $\beta_{mono} = 0$	$I_s = 16.0 \pm 2.1$ GW/cm^2 $\beta_{mono} = 0$
15 layers	$\alpha_{mono} =$ $7.8 \pm 0.9 \times 10^{-5}$ cm^{-1}	$I_s = 7.7 \pm 1.0$ GW/cm^2 $\beta_{mono} = 0.57 \pm 0.06$ cm/MW	$I_s = 7.7 \pm 1.0$ GW/cm^2 $\beta_{mono} = 0$	$I_s = 18.0 \pm 2.3$ GW/cm^2 $\beta_{mono} = 0$
20 layers	$\alpha_{mono} =$ $7.8 \pm 0.9 \times 10^{-5}$ cm^{-1}	$I_s = 8.2 \pm 1.1$ GW/cm^2 $\beta_{mono} = 0.58 \pm 0.06$ cm/MW	$I_s = 8.2 \pm 1.1$ GW/cm^2 $\beta_{mono} = 0$	$I_s = 21.0 \pm 2.7$ GW/cm^2 $\beta_{mono} = 0$

Table S3. Fitting parameters used in the modeling of Z-scans at 535 nm on 5, and superimposed 10-, 15- and 20-layer graphene samples as in Figure S5b and their corresponding plots of $\Delta T/T_0$ vs. I_{00} at $z = 0$ as in Figure S6b.

Fitting Layer Number		——— (red)	— · — (teal)	– – – (blue)
5 layers	α_{mono} = 8.7 ±1.0 ×10^{-5} cm^{-1}	I_s = 11.5 ±1.5 GW/cm^2 β_{mono} = 0.85 ± 0.09 cm/MW	I_s = 11.5±1.5 GW/cm^2 β_{mono} = 0	I_s = 26.0±3.4 GW/cm^2 β_{mono} = 0
10 layers	α_{mono} = 9.1 ± 1.0 ×10^{-5} cm^{-1}	Is = 12.5 ± 1.6 GW/cm2 β_{mono} = 0.81 ± 0.09 cm/MW	I_s =12.5±1.6 GW/cm^2 β_{mono} = 0	I_s = 29.0±3.8 GW/cm^2 β_{mono} = 0
15 layers	α_{mono} = 9.2± 1.1 ×10^{-5} cm^{-1}	I_s = 13.1 ± 1.7 GW/cm^2 β_{mono} = 0.80 ± 0.08 cm/MW	I_s = 13.1±1.7 GW/cm^2 β_{mono} = 0	I_s = 31.0±4.0 GW/cm^2 β_{mono} = 0
20 layers	α_{mono} = 8.9 ± 1.0 ×10^{-5} cm^{-1}	I_s = 14.5 ± 1.9 GW/cm^2 β_{mono} = 0.84± 0.06 cm/MW	I_s = 14.5±1.9 GW/cm^2 β_{mono} = 0	I_s = 35.0±4.6 GW/cm^2 β_{mono} = 0
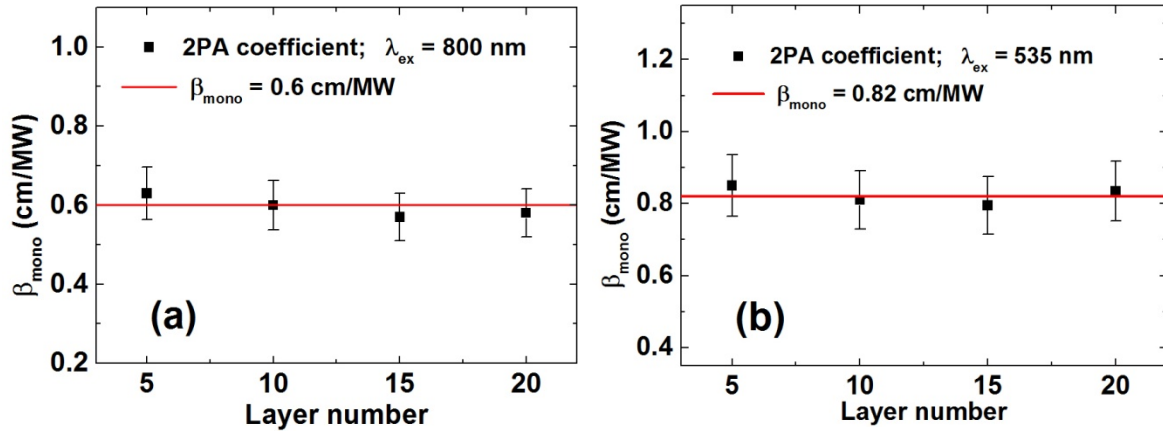
Figure S8. β_{mono} **values measured at 800 nm and 535 nm as a function of layer number.** The black symbols are the obtained β_{mono} values at 800 nm and 535 nm, the solid red lines are guidelines.

REFERENCES

(1) Ferrari, A. C.; Meyer, J. C.; Scardaci, V.; Casiraghi, C.; Lazzeri, M.; Mauri, F.; Piscanec, S.; Jiang, D.; Novoselov, K. S.; Roth, S., et al., Raman Spectrum of Graphene and Graphene Layers. *Phys. Rev. Lett.* **2006**, *97*, 187401.

(2) Reina, A.; Jia, X. T.; Ho, J.; Nezich, D.; Son, H. B.; Bulovic, V.; Dresselhaus, M. S.; Kong, J., Large Area, Few-Layer Graphene Films on Arbitrary Substrates by Chemical Vapor Deposition. *Nano Lett.* **2009**, *9*, 30-35.

(3) Li, X. S.; Cai, W. W.; An, J. H.; Kim, S.; Nah, J.; Yang, D. X.; Piner, R.; Velamakanni, A.; Jung, I.; Tutuc, E., et al., Large-Area Synthesis of High-Quality and Uniform Graphene Films on Copper Foils. *Science* **2009**, *324*, 1312-1314.

(4) Malard, L. M.; Pimenta, M. A.; Dresselhaus, G.; Dresselhaus, M. S., Raman Spectroscopy in Graphene. *Physics Reports* **2009**, *473*, 51-87.

(5) Bae, S.; Kim, H.; Lee, Y.; Xu, X. F.; Park, J. S.; Zheng, Y.; Balakrishnan, J.; Lei, T.; Kim, H. R.; Song, Y. I., et al., Roll-to-Roll Production of 30-Inch Graphene Films for Transparent Electrodes. *Nat. Nanotechnol.* **2010**, *5*, 574-578.

(6) Wu, W.; Yu, Q. K.; Peng, P.; Liu, Z. H.; Bao, J. M.; Pei, S. S., Control of Thickness Uniformity and Grain Size in Graphene Films for Transparent Conductive Electrodes. *Nanotechnology* **2012**, *23*, 035603.

(7) Liao, C. D.; Lu, Y. Y.; Tamalampudi, S. R.; Cheng, H. C.; Chen, Y. T., Chemical Vapor Deposition Synthesis and Raman Spectroscopic Characterization of Large-Area Graphene Sheets. *J. Phys. Chem. A* **2013**, *117*, 9454-9461.

(8)   Pimenta, M. A.; Dresselhaus, G.; Dresselhaus, M. S.; Cancado, L. G.; Jorio, A.; Saito, R., Studying Disorder in Graphite-Based Systems by Raman Spectroscopy. *Phys. Chem. Chem. Phys.* **2007**, *9*, 1276-1291.

(9)   Charlier, J. C.; Eklund, P. C.; Zhu, J.; Ferrari, A. C., Electron and Phonon Properties of Graphene: Their Relationship with Carbon Nanotubes. In *Carbon Nanotubes*; Springer: Berlin/Heidelberg, Germany, **2008**, Volume *111*, pp 673-709.

(10)   Latil, S.; Meunier, V.; Henrard, L., Massless Fermions in Multilayer Graphitic Systems with Misoriented Layers: Ab Initio Calculations and Experimental Fingerprints. *Phys. Rev. B* **2007**, *76*, 201402.

(11)   Lenski, D. R.; Fuhrer, M. S., Raman and Optical Characterization of Multilayer Turbostratic Graphene Grown Via Chemical Vapor Deposition. *J. Appl. Phys.* **2011**, *110*, 013720.

(12)   Faugeras, C.; Nerriere, A.; Potemski, M.; Mahmood, A.; Dujardin, E.; Berger, C.; de Heer, W. A., Few-Layer Graphene on SiC, Pyrolitic Graphite, and Graphene: A Raman Scattering Study. *Appl. Phys. Lett.* **2008**, *92*, 011914.

(13)   Hass, J.; Varchon, F.; Millan-Otoya, J. E.; Sprinkle, M.; Sharma, N.; De Heer, W. A.; Berger, C.; First, P. N.; Magaud, L.; Conrad, E. H., Why Multilayer Graphene on 4H-SiC(000(1)over-Bar) Behaves Like a Single Sheet of Graphene. *Phys. Rev. Lett.* **2008**, *100*, 125504.

(14)   Lespade, P.; Marchand, A.; Couzi, M.; Cruege, F., Caracterisation De Materiaux Carbones Par Microspectrometrie Raman. *Carbon* **1984**, *22*, 375-385.

(15)   Li, X. S.; Zhu, Y. W.; Cai, W. W.; Borysiak, M.; Han, B. Y.; Chen, D.; Piner, R. D.; Colombo, L.; Ruoff, R. S., Transfer of Large-Area Graphene Films for High-Performance Transparent Conductive Electrodes. *Nano Lett.* **2009**, *9*, 4359-4363.

(16)   Sprinkle, M.; Siegel, D.; Hu, Y.; Hicks, J.; Tejeda, A.; Taleb-Ibrahimi, A.; Le Fevre, P.; Bertran, F.; Vizzini, S.; Enriquez, H., et al., First Direct Observation of a Nearly Ideal Graphene Band Structure. *Phys. Rev. Lett.* **2009**, *103*, 226803.

(17)   Blake, P.; Hill, E. W.; Castro Neto, A. H.; Novoselov, K. S.; Jiang, D.; Yang, R.; Booth, T. J.; Geim, A. K., Making Graphene Visible. *Appl. Phys. Lett.* **2007**, *91*, 063124.

(18)   Ni, Z. H.; Wang, H. M.; Kasim, J.; Fan, H. M.; Yu, T.; Wu, Y. H.; Feng, Y. P.; Shen, Z. X., Graphene Thickness Determination Using Reflection and Contrast Spectroscopy. *Nano Lett.* **2007**, *7*, 2758-2763.

(19)   Veshapidze, G.; Trachy, M. L.; Shah, M. H.; DePaola, B. D., Reducing the Uncertainty in Laser Beam Size Measurement with a Scanning Edge Method. *Appl. Optics* **2006**, *45*, 8197-8199.

(20)   Wang, Y. Y.; Ni, Z. H.; Yu, T.; Shen, Z. X.; Wang, H. M.; Wu, Y. H.; Chen, W.; Wee, A. T. S., Raman Studies of Monolayer Graphene: The Substrate Effect. *J. Phys. Chem. C* **2008**, *112*, 10637-10640.

(21)   Bao, Q. L.; Zhang, H.; Wang, Y.; Ni, Z. H.; Yan, Y. L.; Shen, Z. X.; Loh, K. P.; Tang, D. Y., Atomic-Layer Graphene as a Saturable Absorber for Ultrafast Pulsed Lasers. *Adv. Funct. Mater.* **2009**, *19*, 3077-3083.

(22)   Nair, R. R.; Blake, P.; Grigorenko, A. N.; Novoselov, K. S.; Booth, T. J.; Stauber, T.; Peres, N. M. R.; Geim, A. K., Fine Structure Constant Defines Visual Transparency of Graphene. *Science* **2008**, *320*, 1308-1308.

(23)   Mak, K. F.; Sfeir, M. Y.; Wu, Y.; Lui, C. H.; Misewich, J. A.; Heinz, T. F., Measurement of the Optical Conductivity of Graphene. *Phys. Rev. Lett.* **2008**, *101*, 196405.

(24)   Xing, G.; Guo, H.; Zhang, X.; Sum, T. C.; Huan, C. H. A., The Physics of Ultrafast Saturable Absorption in Graphene. *Opt. Express* **2010**, *18*, 4564-4573.

(25)   Zhang, Z.; Voss, P. L., Full-Band Quantum-Dynamical Theory of Saturation and Four-Wave Mixing in Graphene. *Opt. Lett.* **2011**, *36*, 4569-4571.